Journal of Hazardous Materials 448 (2023) 130997

Contents lists available at ScienceDirect

Journal of Hazardous Materials

journal homepage: www.elsevier.com/locate/jhazmat

Research Paper

Ferroptosis is the key cellular process mediating Bisphenol A responses in *Chlamydomonas* and a promising target for enhancing microalgae-based bioremediation

María Carbó [a], Palak Chaturvedi [b], Ana Álvarez [a], Daniela Pineda-Cevallos [c], Arindam Ghatak [b], Pablo Rodríguez González [c], María Jesús Cañal [a], Wolfram Weckwerth [b], Luis Valledor [a,*]

[a] Department of Organisms and Systems Biology and University Institute of Biotechnology of Asturias (IUBA), University of Oviedo, Asturias, Spain
[b] Molecular Systems Biology Lab (MOSYS), Department of Functional and Evolutionary Ecology, University of Vienna, Djerassiplatz 1, 1030 Vienna, Austria
[c] Department of Physical and Analytical Chemistry, University of Oviedo, Asturias, Spain

HIGHLIGHTS

- Chlamydomonas can bioaccumulate significant amounts of Bisphenol A (BPA).
- BPA induced quick oxidative damage in Chlamydomonas, which reverted after 72 h.
- Proteomics revealed the mechanisms involved in BPA detoxification.
- Among them, ferroptosis was the key pathway involved in the initial detoxification.
- Ferroptosis was described for the first time in microalgae and response to BPA.

GRAPHICAL ABSTRACT

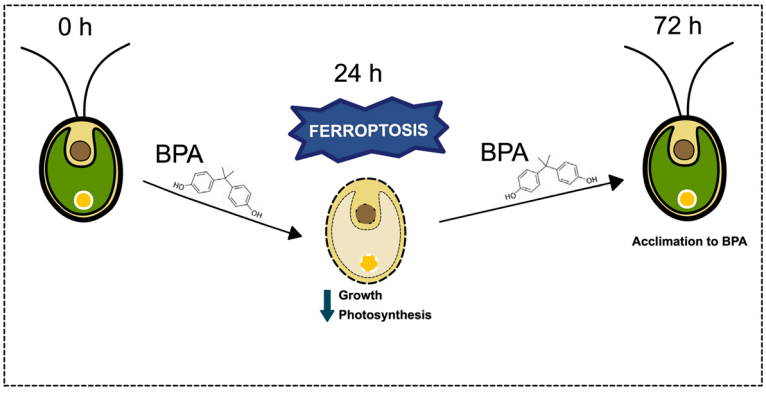

ARTICLE INFO

Editor: Dr. R. Debora

Keywords:
BPA

ABSTRACT

Microplastics are one of the major pollutants in aquatic environments. Among their components, Bisphenol A (BPA) is one of the most abundant and dangerous, leading to endocrine disorders deriving even in different types of cancer in mammals. However, despite this evidence, the xenobiotic effects of BPA over plantae and microalgae

Abbreviations: ACSL, Acyl-Coa synthetase long-chain; AKR1C, Aldoketoreductase type 1C; BCA, Bicinchoninic acid; BPA, Bisphenol A; CAT, Catalase; CEF, Cyclic electron Flow; COX2, Cyclooxygenase 2; $_{dd}H_2O$, Double distilled water; DHODH, Dihydroorotate dehydrogenase; DMSO, Dimethyl sulfoxide; FDR, False discovery rate; FEA1, Low iron-inducible periplasmic protein 1; FEA2, Low iron-inducible periplasmic protein 2; Fer-1, Ferrostatin-1; Fer1, Ferritin heavy chain 1; Fer2, Ferritin 2; FSP1, Ferroptosis Suppressor protein 1; GPX4, Glutathione peroxidase 4; GSH, Glutathione; GSS, Glutathione Synthase; GST, Glutathione S-transferase; HSP90, Heat shock protein 90 chaperone; KOD, Kiss of Death; LIP, Lipid iron pool; LOX, Lipoxygenase; MDA, Malondialdehyde; MnSOD, Manganese Superoxide Dismutase; MSTFA, N-Methyl-N-trimethylsilyl-trifluoroacetamide; PSII, Photosystem II; PUFAs, Polyunsaturated free fatty acids; ROS, Reactive Oxygen Species; SHMT, Serine hydroxymethyltransferase; SOD, Superoxide Dismutase; sPLS, Sparse Partial Least Squares; TSS, Total Soluble Sugars; VDAC1, Voltage-dependent anion channel 1; VDAC2, Voltage-dependent anion channel 2.

* Corresponding author.
E-mail address: valledorluis@uniovi.es (L. Valledor).

https://doi.org/10.1016/j.jhazmat.2023.130997
Received 17 November 2022; Received in revised form 31 January 2023; Accepted 9 February 2023
Available online 12 February 2023

Reactive Oxygen Species (ROS)
Proteomics
Mitochondria
Chloroplast
Xenobiotics

still need to be better understood at the molecular level. To fill this gap, we characterized the physiological and proteomic response of *Chlamydomonas reinhardtii* during long-term BPA exposure by analyzing physiological and biochemical parameters combined with proteomics. BPA imbalanced iron and redox homeostasis, disrupting cell function and triggering ferroptosis. Intriguingly, this microalgae defense against this pollutant is recovering at both molecular and physiological levels while starch accumulation at 72 h of BPA exposure. In this work, we addressed the molecular mechanisms involved in BPA exposure, demonstrating for the first time the induction of ferroptosis in a eukaryotic alga and how ROS detoxification mechanisms and other specific proteomic rearrangements reverted this situation. These results are of great significance not only for understanding the BPA toxicology or exploring the molecular mechanisms of ferroptosis in microalgae but also for defining novel target genes for microplastic bioremediation efficient strain development.

1. Introduction

Human concern about plastic pollution in aquatic ecosystems has been growing in the last few years due to its effects on the environment and human health [1]. Plastics include many different compounds, and among them, Bisphenol A (BPA) 2,2-bis(4-hydroxydiphenyl) propane is one of the most common plastic components. BPA can be found in epoxy and phenolic resins, polycarbonate plastics, and food lacquer coatings [2] as part of daily used products such as thermal receipt paper, lining of cans, or even feeding bottles [3]. Most of the red flags raised by BPA are associated with its disruptor effect on mammals' endocrine system, which could lead to infertility, psychiatric and neurological disorders, and different types of cancer [3]. However, the impact of this xenobiotic might be wider as it can easily reach the aquatic environments arriving at an average of 42.3 ng/L in fresh water [2,3] or even 17.2 mg/L in landfill leachates [4], where it produces similar effects on their inhabitants [5]. Because of this reason, eliminating BPA from the environment is an increasing global concern, and microalgae-based bioremediation seems to be a good alternative as these organisms can assimilate and degrade BPA [6]. Microalgae have many advantages over higher land plants, such as their rapid growth rate, and high rate of atmospheric CO_2 capture, together with no direct competition for agricultural land usage. Nonetheless, to these promising capabilities, BPA induces the microalgae reduction of growth, which leads this strategy to lose attention. Therefore, the generation of new efficient microalgae strains for BPA bioremediation would raise this strategy as a choice. For this, the first step is the characterization at the molecular level of the toxicity of BPA and the microalgae capacity to recover from the induced damage.

Despite the scarce information on the molecular phycotoxic effects of BPA, previous studies demonstrated that green organisms can uptake this compound, showing a range of effects depending on the species and the applied dosages [7]. Even low dosages can induce significant reductions in growth and photosynthetic rates and the disability of reproductive development [8–13]. Despite affecting a vast number of plants and algae, some species are resistant to BPA, showing none or a few changes in their growth and photosynthetic rates as in the algae *Scenedesmus acutus*, *Scenedesmus quadricauda*, *Coelastrum reticulatum*, *Gonium pectorale* and *Cyanophora paradoxa* (10 mg/L of BPA) [14] or even increasing their growth rate in *Chlorella* pyrenoidosa [15], when BPA is applied for long-term. This broad range of responses has been related to the different BPA uptake and antioxidant capacities of the different species. Antioxidant enzymes such are superoxide dismutase (SOD), ascorbate peroxidase and catalase (CAT) are overexpressed during BPA exposure in all microalgae tested [16,17], along with the inhibition of enzymes related to cell respiration in *C. pyrenoidosa* [18]. Together, microalgae such as *Pycocistis sp.* increase the activity of glutathione S-transferase (GST) [17], which is involved in the detoxification of this xenobiotic by its conjugation with glutathione (GSH).

However, at the molecular level, little is known about how BPA disrupts microalgae metabolism or which are the pathways implied in its tolerance, accumulation or biodegradation in those species that are compatible with this pollutant [13,19]. Addressing the molecular level is a necessary step tounderstand the biological effects of this xenobiotic, and identify efficient bioremediation mechanisms, opening the possibility to employ more efficient microalgae to remove BPA from water. Moreover, knowledge of the microalgae response to this plastic could also contribute to understanding the animal response due to the high amount of conserved elements between these two groups [20].

BPA disbalances cell metabolism mainly by increasing reactive oxygen species (ROS) production and the peroxidation of membrane lipids, causing reduced growth and altering normal development. In the last term, lipid peroxidation alters membranes, changing their permeability and affecting the function of chloroplast and mitochondria. This effect was observed by the production of MDA in many Chlorophytes as *C. pyrenoidosa* and *Scenedesmus obliquus* treated with BPA [18]. Also, in other eukaryotic systems mitochondrial and redox damage is observed in mammals producing ferritinophagy, and intracellular iron accumulation is promoted by Fenton's reaction [14] leading to the appearance of ferroptosis [21]. This form of cell death has been described in several prokaryotic [22] and eukaryotic [23–25] systems in response to different stress conditions and has been recently linked to BPA in mammals [26]. However, the physiological and specific biochemical and regulatory mechanisms involved in BPA responses in microalgae are still unknown.

To fill this gap we employed the model organism *Chlamydomonas reinhardtii.* This species was selected over other sensitive (micro)algae or plants [27–30] because of their simple cell cycle, fast growth, the good range of molecular and bioinformatics tools and the ability for bioremediation pollutants already described [31–33]. The combination of proteomics with a physiological characterization during a time-course experiment following a systems biology approach allowed us to describe the short- and long-term effects of BPA over this alga and specific proteins mediating these responses. The initial shock induced by this xenobiotic was mainly caused by a strong redox disbalance which affected a wide range of cellular pathways, mainly at the chloroplast and mitochondrial levels. To resolve this hostile environment, several mechanisms were triggered, being the most important the ferroptosis which was involved in initial detoxification stages. This was the first description of ferroptosis cell death in an eukaryotic microalgae. BPA also induced the accumulation of starch and other metabolites consequently of, the specific rearrangements of biochemical pathways. These findings contribute to understanding the toxic effects of BPA in a cell and to selecting better strategies for plastic bioremediation, providing some candidates for genetic engineering microalgae improvement.

2. Experimental

2.1. Algal strains and culture conditions

Chlamydomonas reinhardtii CC503 (cw92) and CC1690 (Sager strain) were obtained from the Chlamydomonas Resource Center (https://www.chlamycollection.org/). Cells were cultured within a 0.5 L Erlenmeyer flask containing 300 mL of liquid Tris-Acetate-Phosphate (TAP) culture media. Growth conditions were as follows: constant 25 °C temperature, 175 rpm shaking, and a photoperiod of 16:8 (light: darkness) at 200 μmol photon·s^{-1}·m^{-2} provided by warm white LED.

2.2. BPA treatment

Seed cultures were kept growing at an exponential phase and diluted to $5{\cdot}10^4$ cells/mL in TAP before BPA exposition. These cultures were aliquoted in 12 flasks organizing these in four groups of three replicates. Different amounts of a stock of 0.133 g/mL of BPA (Sigma-Aldrich 239658-50G) in methanol (Honeywell, 34885) were added to reach the three different concentrations that were tested (30, 40 and 45 mg/L). Equal volumes of methanol (0.03 % of MeOH) were added to control cultures. For the systems biology-based assay (Supplementary figure 1B), a twelve replicates experiment was set up with two groups of six replicates of 0, controls (0.03 % of MeOH), and 40 mg/L of BPA treatment.

2.3. Ferrostatin-1 treatment

The stock solution of 38 mM of Ferrostatin-1 (Fer-1) (Sigma SML0583) was prepared in DMSO. This solution was added to a final concentration of 1 μM to CC1690 cultures ($5{\cdot}10^4$ cells/mL) 24 h before BPA addition (t − 24 h). The same amount of Fer-1 was added again 1 h before BPA addition (t−1 h). Cultures were then diluted ($5{\cdot}10^4$ cells/mL) and 40 mg/L of BPA final concentration was added to the cultures from a 0.133 g/mL stock prepared in DMSO. The same volume of DMSO was added to control and treatment flasks at t − 24 and − 1 h. Three replicates of each condition were performed.

2.4. BPA determination

Intracellular BPA content was determined by isotope dilution mass spectrometry. Calibration mixtures were performed by adding 100 μL of a 200 μg/g $^{13}C_{12}$-BPA solution to both the samples and the calibration solutions resulting in a concentration of 200 μg/g. The final content of calibration samples was in the range 50–800 μg/g (50, 100, 150, 200, 400, 600 y 800 μg/g). Samples were dried prior to derivatization. Dried samples were dissolved in 20 μL of methoxyamine hydrochloride (Sigma) (40 mg/mL) in pyridine (Sigma), and incubated 30 °C for 90 min. Then, samples were incubated for 37 °C 30 min in 80 μL of MSTFA. Samples were centrifuged for 3 min at 20,000*g* and the supernatant was collected. Finally, the samples were diluted 1:10 with hexane and injected into a GC-TOF system (Agilent 7250). 1 μL of each sample was injected into the GC-Q-TOF system at 230 °C using a 10:1 split ratio. A HP-5MS (30 m × 250 μm × 0.25 μm) capillary column was used for the chromatographic separation. The oven was initially held at 70 °C for 1 min, and the temperature was increased to 76 °C at 1 °C/min and held for 15 min. Then, The temperature was increased to 300 °C at 6 °C/min and held for 5 min. Helium was used as carrier gas at 1.5 mL/min during the chromatographic separation. The source temperature was set at 200 °C. The mass range was set between *m/z* 40 and *m/z* 600. The acquired data were converted into SureMass format before the integration of peak areas for *m/z* 357.1701 (natural BPA) and *m/z* 369.2104 ($^{13}C_{12}$-BPA, TRC-Canada) using the MassHunter Quantitative Analysis 10.2 (Agilent). Using a calibration graph, BPA quantification was carried out by isotope dilution mass spectrometry. Six biological replicates were quantified at each sampling time.

2.5. Photosynthesis and growth rate determination

Cell growth and photosynthesis rate were measured at 0, 5, 24, 48 and 72 h after the experiment onset. Cell growth was monitored by measuring culture absorbance at 650 and 750 nm with Nabi UV/vis Nano Spectrophotometer (MicroDigital Co., Korea). Photosystem II efficiency (Fv/Fm) was measured with a pulse–amplitude modulation fluorimeter (Walz, JUNIOR-PAM) after an acclimation period of 15 min in darkness.

2.5.1. Pigments, malondialdehyde, total soluble sugars and starch content determination

Determination of pigments (chlorophyll A, chlorophyll B and carotenoids), malondialdehyde (MDA), total soluble sugars (TSS) and starch were performed from the same lyophilized extract. At least three replicates for all stress biomarkers were quantified by colorimetry following the protocol and formulae described by López-Hidalgo et al. [34].

2.6. Cell viability and total reactive oxygen species determination

One mL of cells was collected at 0, 5, 24, 72 and 96 h by low-speed centrifugation. For cell viability determination, pellets were resuspended in fluorescein diacetate staining solution (1 mg/mL in acetone) and incubated for 15 min at room temperature in dark [35]. Total reactive oxygen species (ROS) were quantified from the same amount of cultures, pelleted in the same way, employing 2,7-dichlorodihydrofluorescein diacetate (H_2DCFDA, 5 μM) in DMSO solution and incubated for 60 min in dark [36]. Six biological replicates were analyzed at each sampling time.

Both cell preparations were washed twice with $_{dd}H_2O$ to remove the excess of dye, and fluorescence was quantified employing a Qubit 2.0 Fluorometer (Invitrogen) using a excitation/emission wavelengths of 485/530 nm respectively. Cell viability was calculated by the percentage of cells presenting fluorescence under optical fluorescence microscopy (Nikon Eclipse E600). Total ROS in cultures was semi-quantified by considering the ratio of H_2DCFDA/fluorescein acetate fluorescence.

2.7. Perl's staining for intracellular Fe^{3+} detection

Chlamydomonas Fe^{3+} staining was performed as described by Green & Rogers (2004) [37] with slight modifications for microalgae. Briefly, cells were fixed in 4 % (v/v) paraformaldehyde for 60 min and then washed 3 times with $_{dd}H_2O$ for 5 min. Fixed cells were then resuspended in Perl's solution [4 % (v/v) HCl and 4 % (w/v) potassium ferrocyanide] and vacuum infiltrated for 15 min. Finally, cells were washed 3 times with $_{dd}H_2O$ for 5 min and resuspended in water before imaging by optical microscopy (Olympus BX61 coupled to Olympus DP-70 camera) employing a PlanApo 40x/0.95 objective.

2.8. Alcian blue staining for the determination of extracellular matrix

Cultures were collected by low-speed centrifugation as previously described. Cell pellets were carefully resuspended in 1 % formaldehyde and fixed overnight at 4°C. Immediately before staining, cells were centrifuged to remove formaldehyde. Pellets were stained in 0.1 % w/v Alcian blue 8GX in 0.5 N acetic acid and incubated for 10 min at room temperature before microscopy, following the recommendations of Crayton [38]. Images were acquired in a Nikon Eclipse E600 microscope coupled to a Digital Sight DS-5 M camera employing a Pan Fluor 40x/0.75 objective (Nikon).

2.9. Proteomic analysis

Six replicates of Chlamydomonas proteins from 0, 24 and 72 h were extracted from 5 mg of dry weight following the procedure described in Valledor et al. (2014) [39]. Protein pellets were resuspended in 8 M urea and quantified employing BCA [40]. The proteins were pre-fractionated (40 μg of total protein were loaded on to the gel (1D SDS-PAGE)), trypsin digested (Roche No 11418475001) and desalted (using a C18 spec plate) according to a previously described method [41–43]. Before mass spectrometric measurement, the tryptic peptide pellets were dissolved in 4 % (v/v) acetonitrile, and 0.1 % (v/v) formic acid. One μg of each sample was loaded on a C18 reverse-phase column (Thermo scientific, EASY-Spray 500 mm, 2 μm particle size). Separation was achieved with a 90 min gradient from 98 % solution A (0.1 % formic acid in high purity water (MilliQ)) and 2 % solution B (90 % ACN and 0.1 % formic acid) at

0 min to 40 % solution B (90 % ACN and 0.1 % formic acid) at 90 min with a flow rate of 300 nL min^{-1}. nESI-MS/MS measurements were performed on Orbitrap QExactive (Thermo Fisher Scientific, Bremen, Germany) with the following settings: Full scan range 350–1800 *m/z* resolution 120,000 max. 20 MS2 scans (activation type CID), repeat count 1, repeat duration 30 s, exclusion list size 500, exclusion duration 30 s, charge state screening enabled with the rejection of unassigned and + 1 charge states, minimum signal threshold 500.

Raw data were processed with Proteome Discoverer 2.1 (Thermo Fisher Scientific, Bremen, Germany) employing the SEQUEST algorithm [44] and label-free quantified based on precursor's areas. Chlamydomonas 5.6 protein (18750 accessions), Chlamydomonas chloroplast & mitochondria (84 accessions) and UNIPROT-viridiplantae (37821 accessions) databases were employed for protein identification. Only high-confidence proteins (at least one significant peptide, XCorr > 1.8, FDR 5 %) present in all the biological samples of at least one treatment were considered for this analysis.

2.10. Data analysis

Biostatistical analysis was performed in R 4.1.2 (R Foundation for Statistical Computing, Vienna, Austria.) [45] under RStudio IDE (Posit Software, Boston, US) [46]. Preprocessing, univariate and multivariate analyses over proteomic dataset were performed with bundled core packages and pRocessomics (0.1.13) (available at https://github.com/Valledor, University of Oviedo, Oviedo, Spain). Physiological and growth measurements were analyzed employing a t-test or Kruskal Wallis followed by Duncan's. The proteome dataset was first pre-processed, involving imputation, filtering, and balancing steps. Briefly, missing values were imputed only in those cases that they represented less than 17 % of the samples of a particular treatment (one in six replicates) by using the Random Forests algorithm. After imputation, those proteins that were not present in all replicates of at least one treatment or in at least six individual replicates, were filtered out, as they were considered inconsistent. Imputed and filtered data was balanced through a sample-centric approach prior to analysis. As most of the preprocessed protein variables failed to comply with the assumption of normality, we tested for the presence of inter-treatment differences by using the Kruskal Wallis test coupled with the Duncan post hoc test. Heatmaps were conducted, grouping proteins according to MapMan ontology. Sparse Partial Least Squares (sPLS) was employed, considering proteome and physiology/growth datasets as predictive and response matrices respectively. Resulting correlation network was filtered, keeping edges with correlation values above 0.75. The network was visualized and processed in Cytoscape V3.9.1 (Cytoscape Consortium) [47].

2.11. Enrichment analyses

Pathway analysis was conducted employing GO classification. Abundances were visualized employing heatmap representation. Enrichment analyses were performed employing g:Profiler with a custom GMT annotation file parsed from GOMAP following the recommendations provided by [48].

3. Results

3.1. BPA effect on growth depends on the Chlamydomonas cell wall

The growth of two Chlamydomonas strains, CC503 (cell wall defective) and CC1690 (wild type), was monitored for 120 h under different concentrations of BPA (0, 30, 40, 45 mg/L) (Supplementary figure 1*C*, Supplementary table 1). Both strains displayed delayed growth under all tested BPA concentrations (Supplementary figure 1*C*, Supplementary table 1), although the effect was more pronounced for CC1690. Consequently, CC1690 was chosen for further analyses and 40 mg/L of BPA as it allowed enough biomass retrieval during sampling while still producing a stress phenotype (Supplementary figure 1*C*, Supplementary table 1).

3.2. Initial BPA shock caused quick and severe physiological disfunctions

The intracellular level of BPA quickly increased for the first 24 h of exposure, reaching an average concentration of 35.27 μg of BPA/mg of dried cells (Fig. 1*A;* Supplementary table 2). BPA caused a delay in growth (Fig. 1*B*), reduced photosynthetic rate (Fig. 1*C*) and cell death (Fig. 1*D, E*). One of the initial physiological symptoms of BPA intoxication was the disruption of photosynthetic Fv/Fm which was completely blocked after 5 h and later recovered during the time (Fig. 1*C*). This coincided with a fall of photosynthetic pigments (Fig. 1*D, F;* Supplementary table 3), and increased damage to membranes as lipid peroxidation (MDA) raised together with the total ROS content (Fig. 1*E*). After 72 h, BPA concentration decreased in cells to 18.63 μg of BPA/mg of dried cells, while in culture remained the same concentration as in 24 h of treatment (Fig. 1*A;* Supplementary table 2). Pigments started to recover, Fv/Fm reached values similar to controls, and lipid peroxidation was reduced below controls.

Interestingly, while soluble sugars content (Fig. 1*F;* Supplementary table 3) was reduced four times after the initial shock and did not recover during the experiment, starch started to accumulate after 72 h. These responses are accompanied to an induction of BPA Chlamydomonas cell aggregation, also increasing the thickness of the extracellular matrix during the treatment (Supplementary figure 2). After 72 h cells grew exponentially like normal controls (Supplementary table 3).

3.3. Proteomics revealed profound changes in cell biology after BPA exposure

A proteomic approach was performed to explain, at the molecular level, the physiological responses observed after BPA treatment up to 72 h. Longer culture periods were not assayed as the cultures behave similarly to controls. The analysis of whole-cell proteome revealed more than 3000 proteins, but only 2158 were confidently identified and semi-quantified considering search and abundance thresholds (Supplementary table 4*)*. Within these proteins, 1822 proteins (84.43 %) showed significative differences in at least one treatment (Kruskal-Wallis, q-value <0.05), indicating the profound proteome change induced by BPA.

To obtain a comprehensive picture of the physiological disruption induced by BPA, proteins were firstly classified according MapMan ontology employing Mercator tool [49] and annotating 1408 to functional bins. A heatmap analysis and cluster classification of the different treatments according to these bins (Fig. 2*A;* Supplementary figure 3) revealed that the initial BPA shock caused an up-accumulation of chromatin organization and DNA repair mechanisms, signalling (phytohormone action, external stimuli response), solute transport and protein biosynthesis. In contrast, almost all other bins were down-regulated. After 72 h of BPA exposure, samples were grouped with controls rather than with the samples of 24 h BPA, indicating the recovery of these cultures. Most bins recovered to control abundances, except for phytohormone action, DNA damage response, and protein biosynthesis, which were still above control values despite reducing their abundance. The minor changes observed within controls reflected the normal growth of the culture and the increasing concentration of cells within flasks.

However, within these major bins, differential protein abundance patterns were found. Sixteen co-accumulation patterns were defined after a k-means analysis (Fig. 2*B;* Supplementary table 5). Again, the most abundant differences between control and treated cultures were found at 24 h. Four clusters (6, 11, 13 and 15; 451 proteins) classified the proteins which quickly responded to BPA and then returned to control levels. The function of these clusters was inferred after a

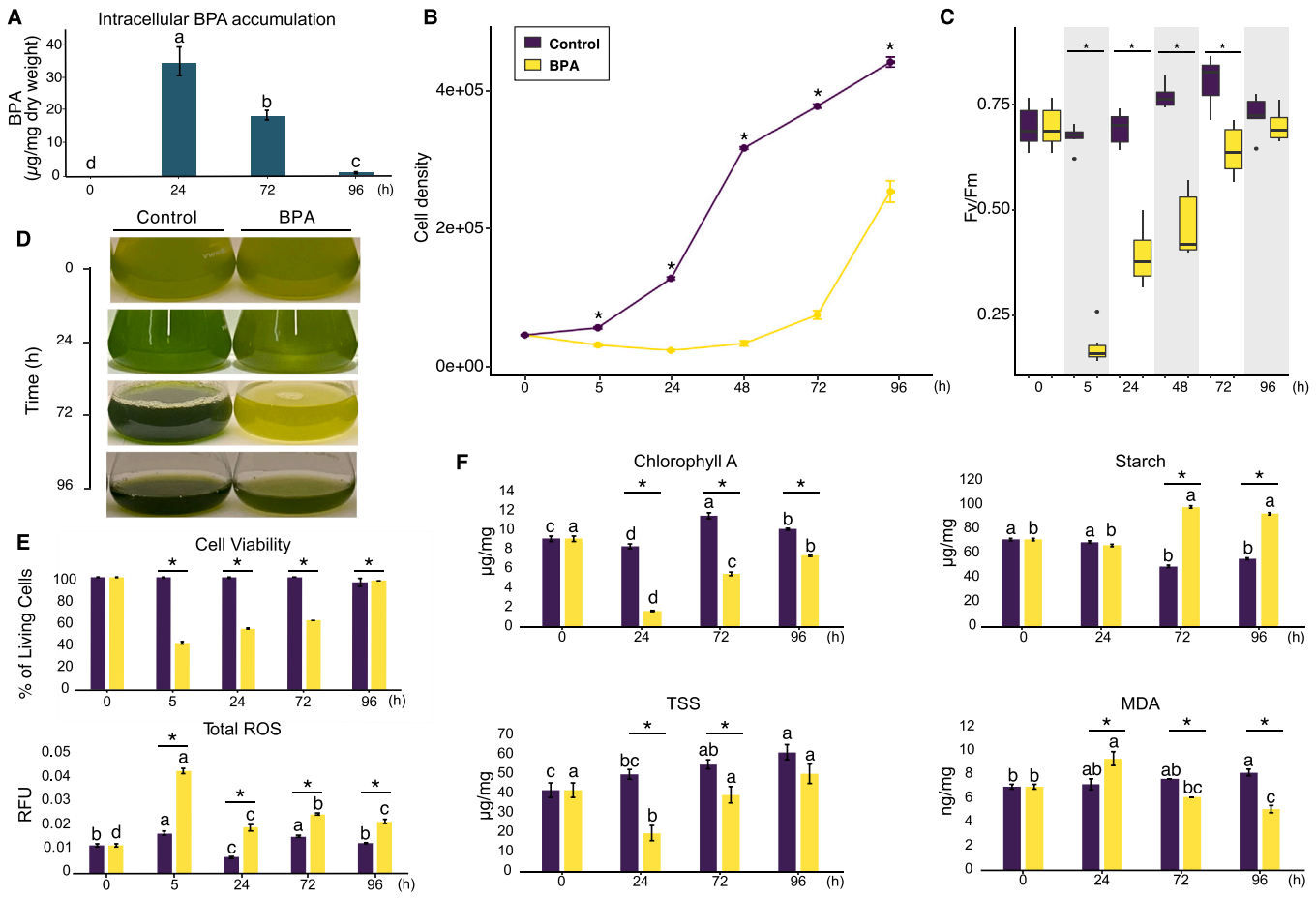

Fig. 1. Proteomic assay results for BPA intracellular accumulation (A) growth rate (B), Fv/Fm (C), the aspect of the growth during time (D), cell viability percentage and the total ROS (E), chlorophyll A, starch, TSS and MDA measures (F). Different letters indicate significant differences between sampling times within each group (controls or BPA). Asterisks indicate significant differences ($p < 0.05$) between BPA and controls respectively at each sampling time.

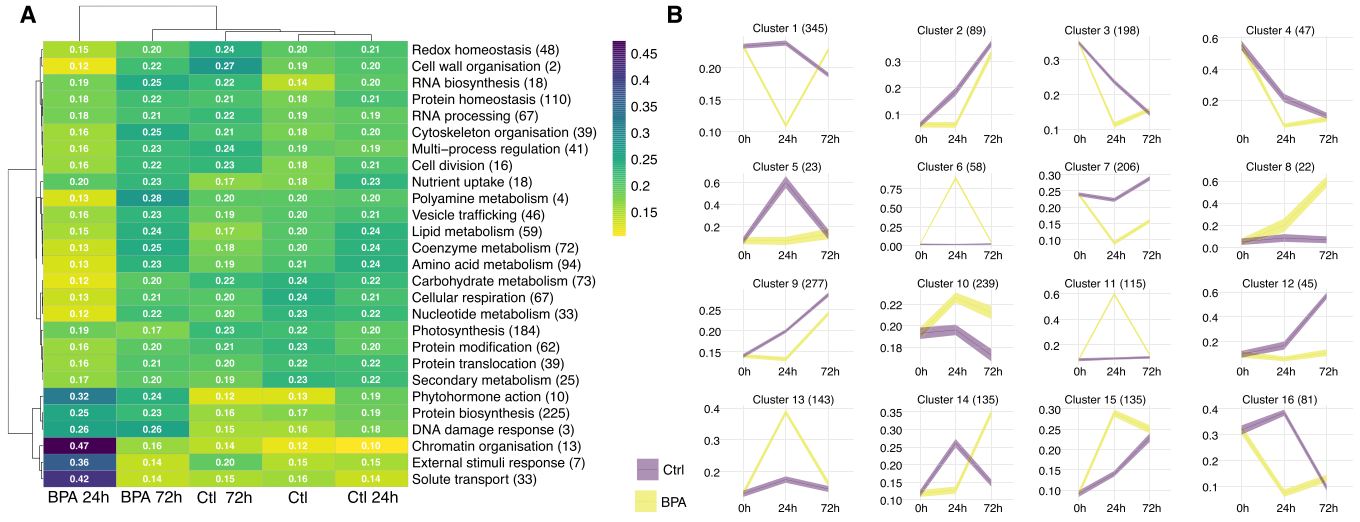

Fig. 2. Proteomic results for control and BPA treatments during 72 h. Proteins separated into MapMan categories heatmap (A), k-means clustering analysis (B).

functional enrichment analysis employing secondary and tertiary bin levels (Supplementary figure 4), revealing that redox homeostasis, photophosphorylation of PSII and ATP synthase complex, plastidial, LSU and SSU ribosome biogenesis, and U2-RNA processing pathways were upregulated after the initial shock caused by BPA. Two clusters (8, 10; 261 proteins) classified those proteins over-accumulated at 24 and 72 h and were enriched in photophosphorylation of PSII and ATP synthase complex, protein biosynthesis and homeostasis, and one (14; 135 proteins) those proteins over-accumulated after 72 h, which was enriched in fatty acid degradation, carotenoid biosynthesis, protein biosynthesis and nutrient uptake. On the other hand, most of the clusters that showed initial down-accumulation (clusters 1, 2, 3, 4, 5, 16; 783 proteins)

recovered after 72 h of culture and were enriched in a range of cellular processes from the Calvin cycle, carbohydrate, lipid, protein or amino acids metabolism (SHMT pathway) to cellular respiration or protein translocation. Finally, clusters 7, 9, and 12 (528 proteins) gathered those proteins down-accumulated during the experiment and showed a similar enrichment to the previous group, with the noticeable inclusion of redox homeostasis (SOD and thiol-based redox regulation).

3.4. Multivariate analyses revealed the redox homeostasis is disbalanced in response to BPA

sPLS was employed to discover those proteins more related to the observed variations at the physiological level. This method adequately distinguished the different treatments and showed that component 1 gathered most of the variation related to BPA treatment (Fig. 3*A*). As in previous analyses, cultures after 24 h of BPA exposure were the most different samples, while the cultures recovered after 72 h were grouped with controls. The functional enrichment analyses of top positively and negatively correlated proteins to component 1 (Fig. 3*B*) revealed that BPA induced protein biogenesis at chloroplast and reticulum levels, U2-mediated RNA processing and PSI and II after 24 h of culture, supporting k-means-based findings. On the other hand, BPA diminished carbohydrate metabolism, Calvin-Benson cycle, cell respiration and lipid metabolism, N-related pathways, and redox homeostasis, recovered after 72 h. Interestingly, in the case of the Photosystem I term, which was enriched both positively and negatively, those components related to iron-sulfur centre or ferredoxin interaction were upregulated. At the same time, -harvesting complexes and their docking proteins were downregulated. Out of these clusters, proteins related to iron uptake, cell wall, and voltage gate ion channels were positively correlated to this component (Supplementary table 6).

A protein-physiology data correlation network was also defined from the sPLS regression (Fig. 4). This network revealed that photosynthesis proteins are positively related to Fv/Fm, growth, chlorophyll A and B and total soluble starch. Together, are positively correlated elements related to redox homeostasis (MnSOD) and lipid metabolism proteins to chlorophylls, TSS and Fv/Fm. Moreover, some carbohydrate metabolism proteins are positively linked to Fv/Fm and chlorophyll A. This network also revealed epigenetic mechanisms in BPA Chlamydomonas response, as Argonaute appeared positively related to growth. On the other hand, protein synthesis is negatively correlated to all physiology data, along with carbohydrate metabolism nodes that are negatively linked to TSS, Fv/Fm and chlorophyll B. Also, the enzymes corresponding to redox homeostasis malic enzyme and a sulfiredoxin are negatively linked to chlorophyll A and Fv/Fm.

3.5. BPA-induced major changes in carbon metabolism

The observed reduction of soluble sugars and the accumulation of starch could result from reduced photosynthesis and cellular respiration. The decay of the Fv/Fm was coincident with the loss of antenna proteins, core photosystems proteins, and the reduction in the photosynthetic pigments. At the same time, some iron-related proteins associated with the electron flow over-accumulated, and ferredoxin-NADP-reductases decreased their abundance 2 to 4-fold.

Besides, protein isoforms such as Chlorophyll a-b binding protein 2 (P08963), the Photosystem I iron-sulfur centre (P06251) and a Photosystem II CP47 reaction centre protein (Q9MUV7) were only detected during the initial shock (Supplemental table 4). Contrary to core photosystem proteins, carbon fixation enzymes reduced their abundance, being the sum of all RuBisCO large subunit and RuBisCO activase isoforms, and sedoheptulose-1,7-bisphosphatase (Cre03.g185550) reduced to − 2-, − 1.5- and − 2.5-fold respectively. RuBisCO large subunit deficient mutants displayed enhanced cyclic electron flow (CEF) in Chlamydomonas [50], enhancing ATP production and reducing NADPH synthesis. This fact, together with the reduction of the abundance of some acetyl-CoA carboxylases and synthases, the malate synthase and some isocitrate lyases may lead the ATP production to stimulate starch synthesis, accumulated under BPA 72 h (Fig. 1*F*, Supplementary table 3).

Protein biosynthesis was the main enriched category after 24 h of BPA (Fig. 3*B*) and within them, especially those related to plastidial ribosome biogenesis. This might reflect a profound chloroplast proteome turnover after the initial BPA shock, being the first step to recuperating, which is also occurring at cytosol level as proteins associated with large and small ribosomal subunits, which might drive protein remodelling, were also enriched.

Cellular respiration may not to be a sink for imported acetate, as glycolysis, pyruvate oxidation, and tricarboxylic acid pathways decrease. Moreover, some acetyl-CoA carboxylases and synthases, the malate synthase and some isocitrate lyases decreased, probably because they are the rate-limiting enzymes for fatty acid synthesis [51],

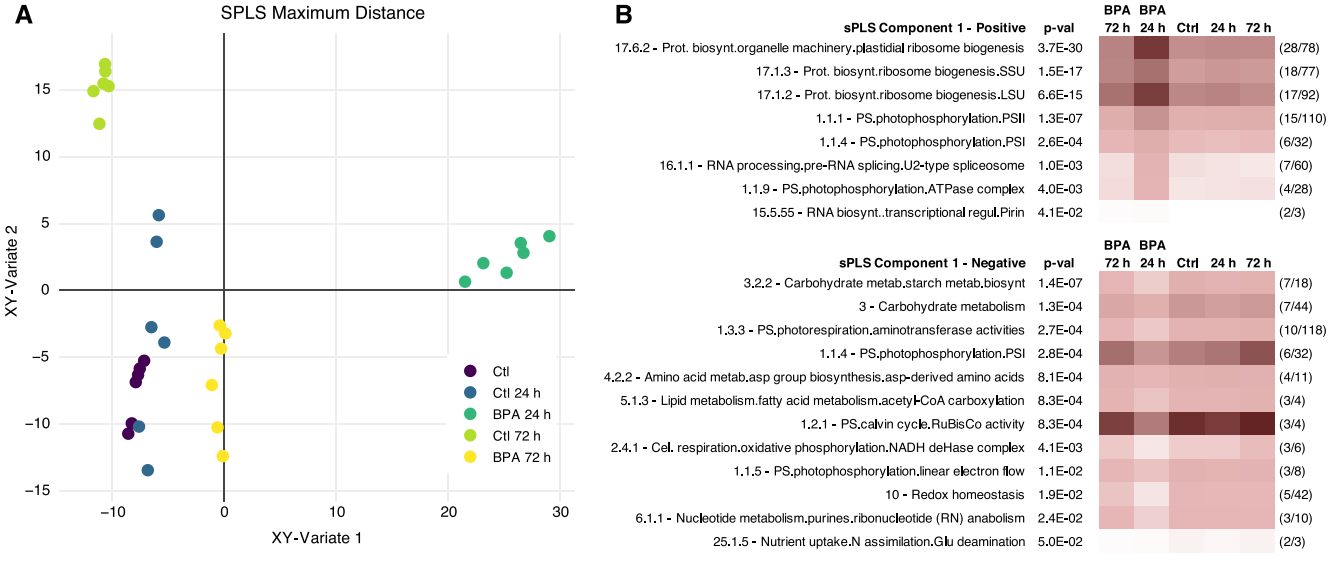

Fig. 3. Integration sPLS of proteins and physiology measurements (growth, Fv/Fm, MDA, starch, TSS, chlorophyll A (ChlA), chlorophyll B (ChlB) and total phenolic content (TPC) (A) and protein enrichment aggrupation into MapMan categories (B).

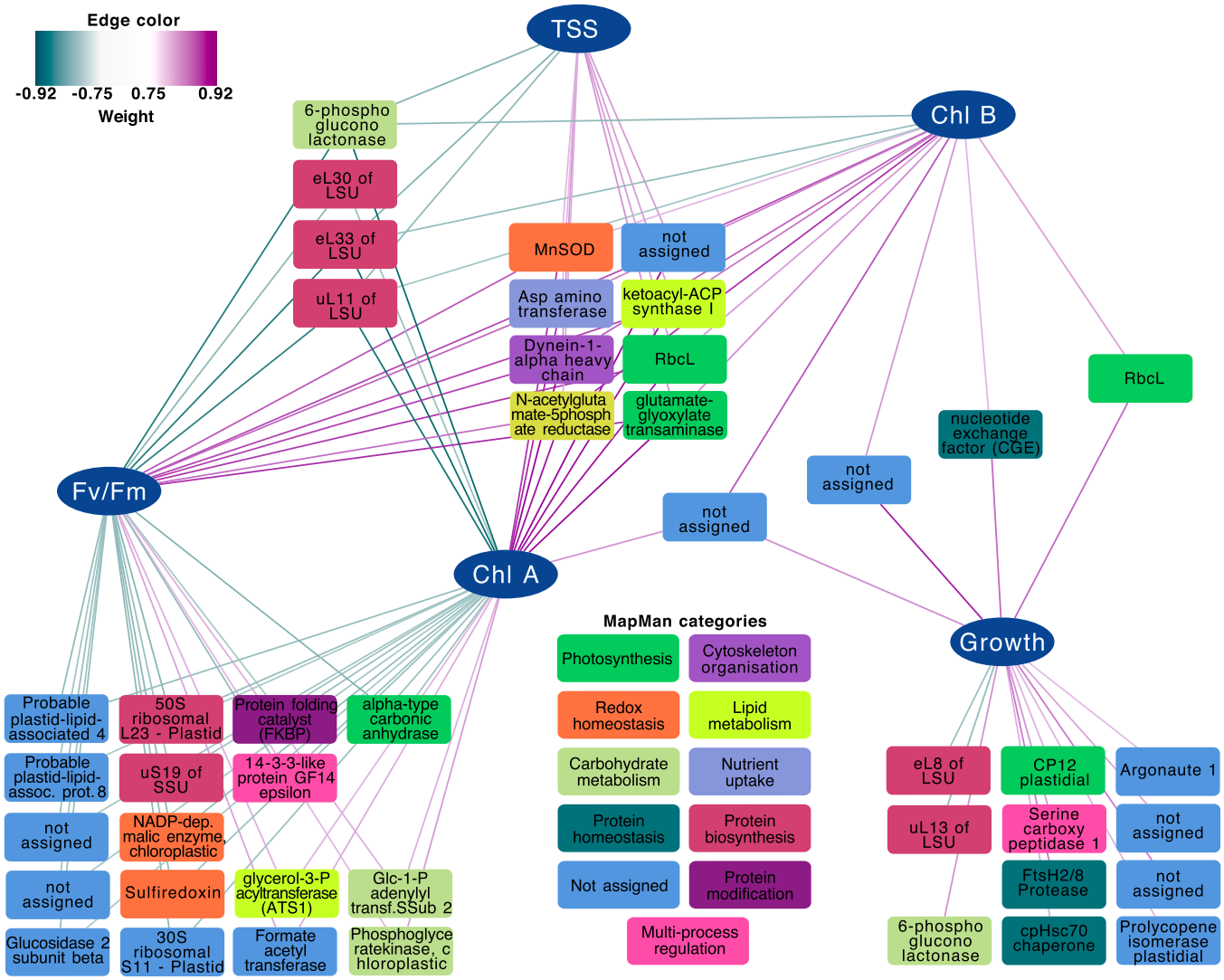

Fig. 4. Integration sPLS resulting network of proteins, growth, Fv/Fm, MDA, starch, TSS, chlorophyll A (ChlA), chlorophyll B (ChlB) and total phenolic content (TPC).

contributing to lipid peroxidation prevention. The misbalance in photosynthesis and CEF production, the reduced cellular respiration and acetyl-CoA carboxylases might drive the ATP production to the starch synthesis to ensure carbon supply for central metabolism (Fig. 2*A*) [28,29,52]. Starch is the most common Chlamydomonas sugar accumulated under stress (Fig. 1*F*). It was not a direct result of increased accumulation of biosynthetic enzymes but to a reduction of amylases (−3.3-fold after 24 h of BPA exposure). After 72 h of BPA exposure, cells recovered abundances similar to the control.

3.6. *BPA imbalanced Iron and redox homeostasis*

ROS (Fig. 1*E*) sharply increased after 5 h and proteins involved in ROS scavenging and lipid peroxidation accumulated 24 h after the start of BPA treatment, which was coincident with a reduction in total ROS. The Chlamydomonas Linoleate 9S-lipoxygenase and COX2 reached their abundance peak at t 24 h (Table 1), and enzymatic lipid peroxidation final product, MDA, reached a maximum after 24 h of BPA exposure.

ROS detoxification-related proteins also accumulated under 24 h of BPA treatment, including Mn superoxide dismutase, monodehydroascorbate reductase 5 (Q84PW3, only present in this time), sulfiredoxin, glutathione peroxidase, thiosulfate sulfurtransferase, rhodanese and Glutathione-S-Trasferase (Cre17.g742300) (Table 1). On the other hand, enzymes involved in GSH synthesis as GSH synthase, gamma-glutamyl cysteine synthase and SHMT showed reduced abundance under BPA treatment. Two aldoketoreductase type 1 C involved in the detoxification of lipid active species [53], also showed a decrease in abundance at t 24 h on BPA treated cultures.

As mentioned above, a variation in the accumulation in proteins related to iron as well as their economy, such are the iron-sulfur center clusters and ferredoxins is taken place under BPA treatment. The iron homeostasis-related proteins FEA1, FEA2, and Fer1 and Fer2 (Table 1) also accumulated in Chlamydomonas after 24 h BPA addition. Furthermore, BPA also induced the accumulation of Fe^{3+} clusters (Fig. 5*D*) in Chlamydomonas. This microalga commonly store iron in its ferrous form. Spontaneous intracellular reactions known as Fenton reactions between a large H_2O_2 pool and Fe^{2+} generate large amounts of reactive -OH and Fe^{3+}. Moreover, the iron-binding human homologue pirin proteins (Table 1) accumulated under BPA treated cultures.

The alteration in the oxidation state of iron, promoted by the occurrence of Fenton reaction, together with ROS enhancement and lipid peroxidation were recently associated to ferroptosis [24,25,54,55], a mitochondrial driven process of cell death. Results suggested that BPA triggered ferroptosis. This hypothesis was supported, among others, by the altered abundances of lipid peroxidation related proteins (and increased MDA), iron homeostasis and ROS detoxification proteins

Table 1
List of ferroptosis related biomarkers modulated by BPA treatment. BPA-24 h-C-24 h and BPA-72 h-C-72 h data come from posthoc analysis.

Protein ID	Description	Log2 FC 24 h	Log2 FC 72 h	q-value (Kruskal-wallis)	BPA-24 h - C-24 h	BPA-72 h - C-72 h
Cre12.g546550	FEA1	4.84	0.75	0.005	0.012	0.251
Cre12.g546600	FEA2	3.10	-2.18	0.001	0.006	0.082
Cre09.g387800	Fer1	1.62	-0.08	0.001	0.000	0.577
Cre01.g033300	Fer2	3.57	0.09	0.002	0.000	0.922
Cre01.g028850	Rhodanese	1.60	1.77	0.005	0.011	0.624
Cre01.g022500	NADP-Malic enzyme	> 10	0.00	0.000	–	1.000
Cre12.g555803	Human FSP1 homolog	< 10	1.79	0.164	–	0.336
Cre16.g676150	Mitochondrial MnSOD	6.98	0.78	0.002	0.000	0.767
Cre13.g584850	Glutathione S-transferase	-4.36	-0.66	0.043	0.002	0.707
Cre16.g680454	Glutathione S-transferase	2.14	4.55	0.001	0.116	0.000
Cre03.g154950	Glutathione S-transferase	1.78	2.76	0.002	0.085	0.001
Cre12.g538100	Glutathione S-transferase	> 10	1.40	0.096	–	0.195
Cre16.g688550.	Glutathione S-transferase	2.60	1.47	0.001	0.001	0.088
Cre17.g742300	Glutathione S-transferase	2.48	0.18	0.001	0.000	0.376
Cre12.g553700	Glutathione S-transferase	1.90	1.59	0.001	0.002	0.010
Cre15.g636800	Glutathione S-transferase	-1.10	1.47	0.001	0.009	0.003
Cre03.g199423	Dihydroorotate dehydrogenase	< 10	-0.30	0.001	–	0.392
Cre10.g458450	Glutathione peroxidase	1.23	1.68	0.001	0.004	0.011
Cre17.g708800	Glutathione synthase	-1.89	-0.22	0.036	0.008	0.512
Cre02.g077100	Gamma-glutamylcysteine synthetase	-2.16	-0.17	0.001	0.000	0.376
Cre05.g241950	VDAC2	3.13	0.06	0.007	0.009	0.533
Cre01.g013700	VDAC1	1.98	-0.50	0.001	0.001	0.049
Cre12.g507400	ACSL	< 10	> 10	0.033	-	-
Cre13.g566650	ACSL	-2.05	-0.65	0.002	0.000	0.088
Cre03.g182050	ACSL	-1.53	0.31	0.018	0.010	0.646
Cre13.g566650	ACSL	-2.05	-0.65	0.002	0.000	0.088
Cre09.g386750	HSP90 chaperone	1.68	0.71	0.001	0.002	0.168
Cre17.g724150	Human Drp1 homolog	-4.46	0.51	0.001	0.000	0.308
Cre03.g190850	Enoyl coenzyme A hydratase 1	1.34	-1.53	0.019	0.030	0.462
Cre17.g729950	Sulfiredoxin	3.13	1.98	0.001	0.002	0.519
Cre10.g432900	Aldo-keto reductase type 1 C (AKR1C)	-1.30	1.19	0.036	0.066	0.049
Cre12.g518900	Aldo-keto reductase type 1 C (AKR1C)	-1.66	0.04	0.003	0.002	0.670
Cre12.g512300	Linoleate 9S-lipoxygenase (LOX)	0.77	0.67	0.021	0.015	0.015
Cre01.g049500	Cicloxygenase 2 (COX2)	0.69	-0.41	0.001	0.000	0.022
Cre16.g664550	SHMT	-1.01	-0.80	0.001	0.001	0.018
Cre16.g674964	Transcriptional co-regulator (Pirin)	3.34	4.33	0.001	0.001	0.001
Cre09.g388208	Transcriptional co-regulator (Pirin)	> 10	> 10	0.000	0.001	0.001

(Table 1).

3.7. Ferroptosis inhibitor Fer-1 alleviates BPA stress

To support the outcome of the proteomic results that BPA triggered ferroptosis cell death in Chlamydomonas, we next cultured with a ferroptosis inhibitor and BPA to assess its effect. Among canonical ferroptosis inhibitors, Fer-1 protects cell over membrane lipid peroxidation inhibiting this type of cell death. The preventive effect of Fer-1 over lipid peroxidation occurs at t 24 h, as MDA has no difference to control conditions (Fig. 5*C*, Supplementary table 7). Chlamydomonas treated with Fer-1 and BPA recuperate better in the first 24 h of treatment (Fig. 5*A, B, C, D*) compared to cultures with BPA treated ones in both photosynthesis and growth rate (Supplementary table 7). Regarding photosynthetic pigments, Fer-1 BPA mitigation appeared in chlorophyll A, as their amount didn't go down as much as in BPA-treated ones (Fig. 5*C*, Supplementary table 7). Also, starch is lower in Fer-1 BPA-treated cultures than in BPA-treated ones (Fig. 5*C,* Supplementary table 7), indicating a fast recovery. This fast recovery of Fer-1 seemed to alleviate Fe^{3+} accumulation at 72 h of BPA treatment (Fig. 5*D*) matches to the rest of the results, implying Fenton reaction is reduced compared with BPA-treated cultures.

4. Discussion

Plastic pollution, including BPA, is a reality we cannot hide. At the environmental scale, BPA had strong developmental effects over a wide range of land and aquatic taxa affecting their developmental patterns [56]. Despite its relevance, the molecular effects of BPA are only well known in mammals, most of them are a consequence of a metabolic disruption [3]. In photosynthetic organisms, the effects of this xenobiotic at the molecular level have been poorly described, especially in aquatic species [31,57]. In this work, we aimed to shed light on the molecular mechanisms mediating BPA response in the model microalgae *Chlamydomonas reinhardtii*, which showed a significant BPA extractive capacity. We systematically evaluated physiological and proteome-based responses employing a comprehensive approach and described the capability of this organism for bioremediation.

At the physiological level, Chlamydomonas responded to high concentrations of BPA, like land plants. The initial shock, which caused photoinhibition in Chlamydomonas and reduced pigment contents, was previously described in soybean [58] and is probably a consequence of increased membrane damage and reduced antioxidant machinery, as reported in Oryza [7]. The accumulation of reactive oxygen species could also increase the turnover of the active centre of PSII, as D1 protein was over-accumulated, increasing the photoinhibition effects of BPA as reported in cucumber [59]. The consequent decrease of reduced ferredoxin and NADPH may inactivate key enzymes of the Calvin Cycle, reducing carbon fixation and soluble sugars. As in land plants [10,57], BPA also triggered the accumulation of proteins related to hormone signalling in Chlamydomonas, highlighting those related to ABA, a well-known stress mitigator in this species [60,61]. After longer incubation times, coincident with the recovery of the cell function and the reduction of the intracellular BPA, these pathways returned to control values.

However, little is known about the specific molecular mechanisms mediating the recovery of cultures and the accumulation and detoxification of BPA. As in many other stresses in this alga [28–30], the required metabolic rearrangement towards survival was a consequence of the reprogramming of chromatin, the importance of Argonaute

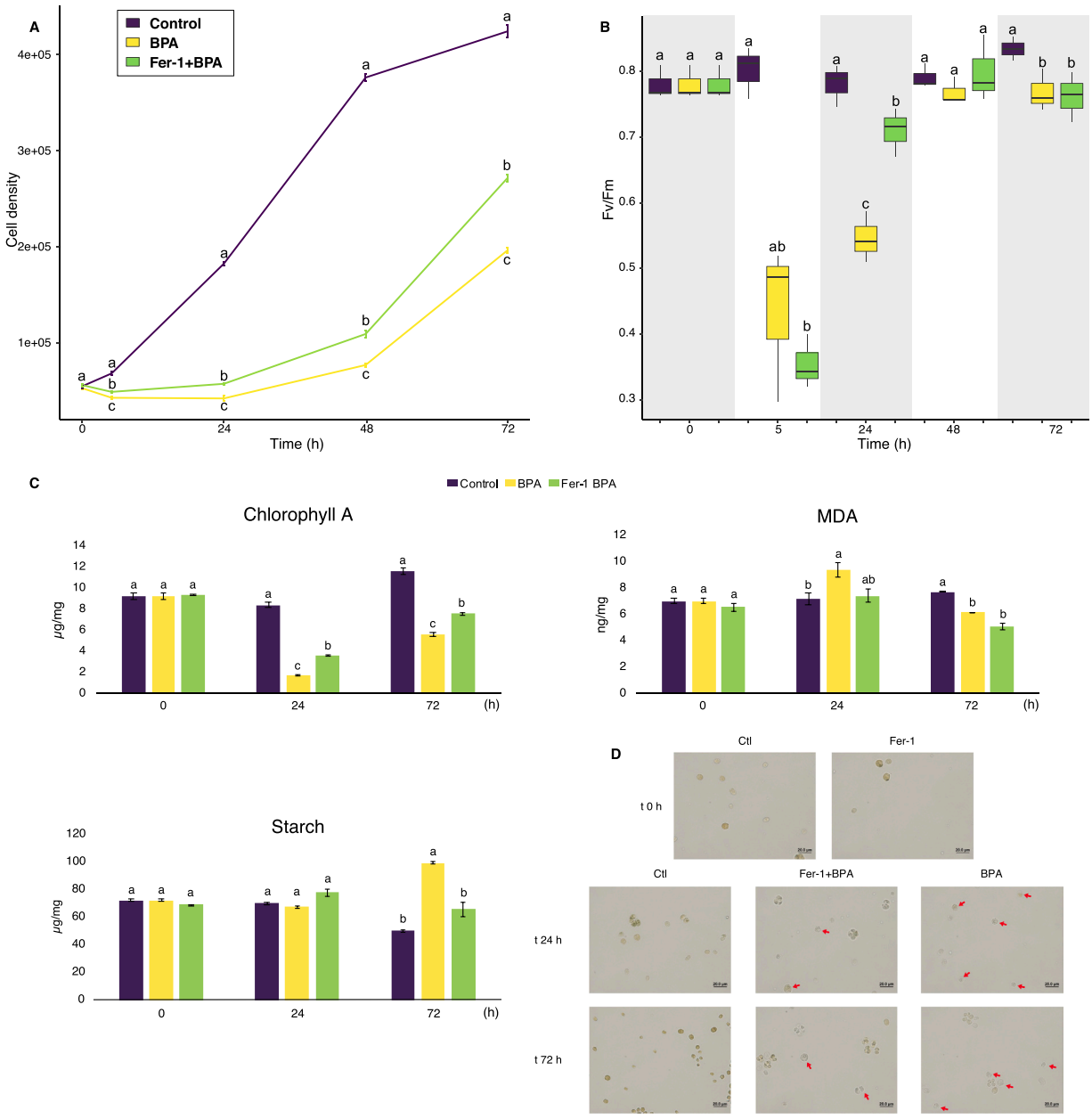

Fig. 5. Growth rate (A), Fv/Fm (B) and stress biomarkers content: chlorophyll A, MDA and starch (C) regarding to control, BPA and Fer-1 +BPA treatments during 72 h. D) Perl's Blue precipitates for Fe^{3+} in cell microscopy images for control, BPA and Fer-1 +BPA treatments during 72 h. Different letters indicate significant differences ($p < 0.05$).

protein revealed the significance of epigenetic mechanisms and, consequently, the synthesis of new proteins by the BPA influence on post-transcriptional regulation of gene expression by miRNAs. Argonaute relevance under BPA treatment has also been reported in mammals, as this xenobiotic might influence miRNA processing [4]. Most of the responses to BPA may be triggered by independent inputs, such as redox state and NADPH availability, C/N ratios, and cell damage among others [29,52], being part of the common stress responses, which combined represent a specific algal response.

The first line of defense in Chlamydomonas would try to limit the amount of BPA introduced in the cells. BPA first induced the aggregation of cells forming multicellular structures that protect part of the cells, as also has been reported under other plastic stress, such as polystyrene microplastics [62]. Moreover, the extracellular matrix was also thickened due to the overaccumulation of matrix-related proteins. These proteins probably act as a stronger barrier to the intracellular diffusion of BPA. However, these mechanisms cannot fully protect cells, as they intake BPA as a second line of defense step for reducing this xenobiotic toxicity.

In land plants, this xenobiotic can be inactivated by direct conjugation with GSH by the action of GST [63]. As GST was accumulated after 24 h of exposure, Chlamydomonas may also employ this strategy to neutralize BPA and allow its intracellular accumulation, as already been demonstrated in other microalgae species [13,19], and may explain the observed intracellular reduction of free BPA after 72 h of culture. As a counterpart, this new sink of GSH would lead to a weak capability for neutralizing ROS, that is highly accumulated during all BPA treatment. In animals, plants and yeast BPA exposure produces redox disbalance and increase ROS production leading to changes in mitochondrial membrane permeability and potential [64–67]. Animal sulfiredoxins control intracellular ROS by engaging in H_2O_2 signaling throughout the overoxidation of 2-cys peroxiredoxins [68]. The sequence of the

Chlamydomonas sulfiredoxin is closer to their plant than to their plant orthologs. Enzymes involved in the recycling and transfer of GSH serve as double purposes: control ROS levels by transferring reducing power to diverse ROS detoxification mechanisms and by directly detoxifying BPA via its conjugation with GSH. This situation could lead to the observed conversion of Fe^{2+} to Fe^{3+}, inducing a ROS and Fe^{3+} dependent cell death during the first stages of BPA exposure consequence of mitochondrial membrane damage, hypothesis supported by the recent description of increased lipid peroxidation in mitochondria caused by BPA [26]. The presence of a pirin a protein which, in humans, acts as nuclear redox sensor and regulator [69,70] and is activated by Fe^{3+} accumulation uphold the iron misbalance. Moreover, the iron unbalance may be also present in the chloroplast, as the accumulation of iron-related proteins associated with the electron flow together with the decreasing accumulation of ferredoxin-NADP-reductases suggest some iron-related and/or redox imbalance, as iron essential for electron transfer chain in both mitochondria and chloroplast membranes. Under iron deficiency, Chlamydomonas has a large proportion of redox related transcripts, associated to compromised PSI [71]. Furthermore, some proteins that accumulate under iron deficiency accumulated under BPA 24 h of treatment. FEA1 and FEA2 [72,73] that are algal specific proteins involved in ferrous iron assimilation, and Fer1 and Fer2 ferritins and are chloroplast iron chelators, supporting our hypothesis.

The combination of reduced GSH, iron oxidation and lipid peroxidation suggested the occurrence of ferroptosis (Fig. 6). This is not the first time a xenobiotic is related to ferroptosis as the herbicide (R)-Dichlorprop induced ferroptosis in *A. thaliana*, atrazine in rat brain [74], or Paraquat in humans [75], but this is the first time that BPA is related to this process in a photosynthetic organism, and the also first time in which ferroptosis has been described in microalgae. Despite BPA-induced ferroptosis has not been described in photosynthetic organisms, in plants ferroptosis was first described under heat stress [22,76] and pathogen immune response [77]. In Arabidopsis, ferroptosis-triggered heat stress induces a lack of GSH for an unknown reason, leading to a Glutathione peroxidase 4 (GPX4) inhibition [76,78]. These works also proposed the increase of voltage-dependent anion channels (VDAC), up-accumulated by Chlamydomonas after BPA exposure, as necessary Ca^{2+} transporters for heat-induced ferroptosis [76]. BPA treatment may oligomerize these pores altering mitochondrial Ca^{2+} permeabilization and decreasing NADH oxidation (Fig. 6). All these might cause the increase of ROS, including H_2O_2 that GPX could not detoxify as GSH is not available because it is used by GST to BPA detoxification (Fig. 6). The accumulation of H_2O_2 might react with Fe^{2+} and by Fenton's reaction creates reactive -OH and Fe^{3+}, which might

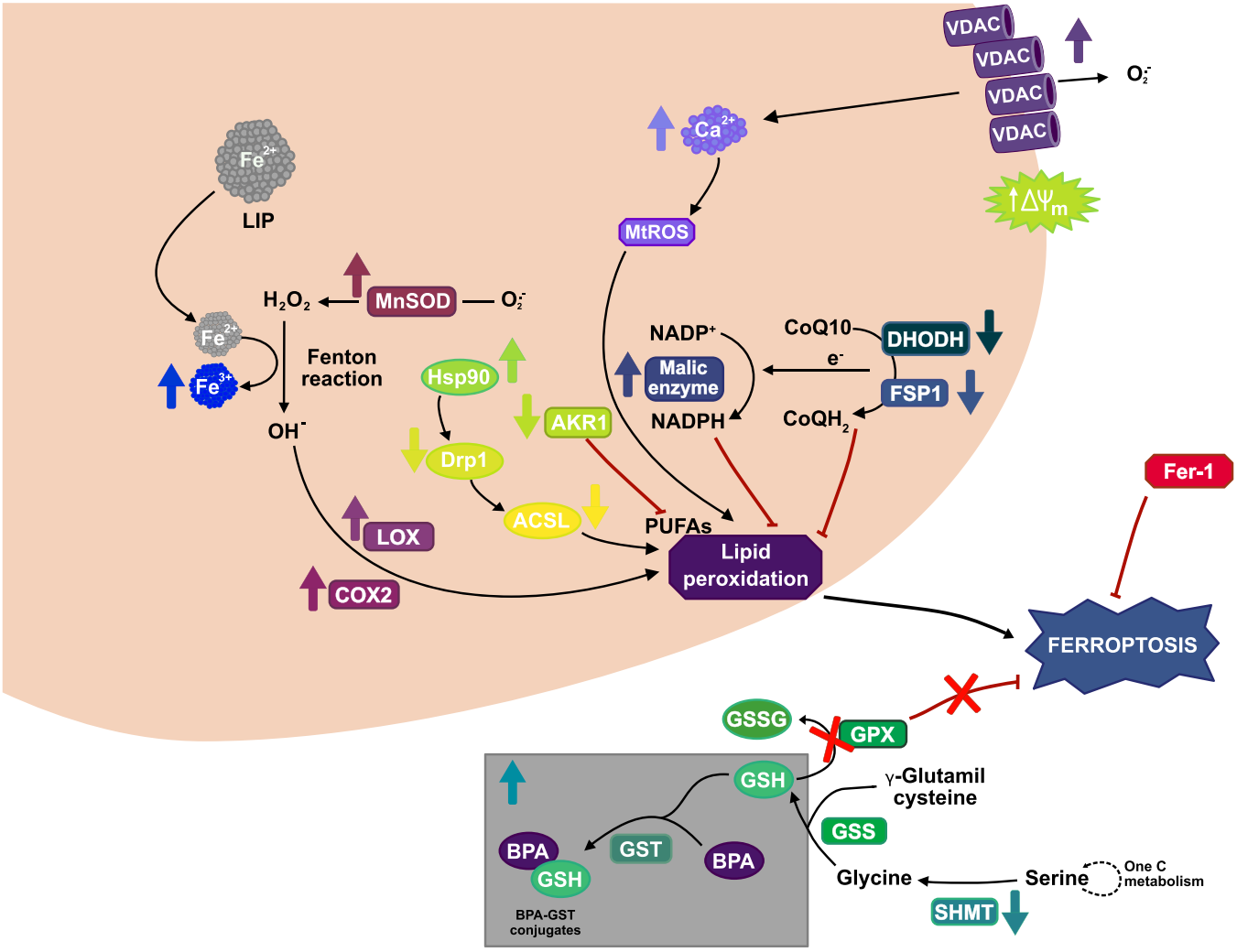

Fig. 6. Proposed hypothesis of the proteins involved in ferroptosis induced by BPA at 24 h of treatment in Chlamydomonas. VDAC: voltage anion channels; MtROS: mitochondrial ROS; LIP: lipid iron pool; MnSOD: Mn superoxide dismutase; LOX: lipoxygenase; COX2: cyclooxygenase 2; HSP90: heat shock protein 90 chaperone; Drp1: dynamin-related protein 1; ACSL: Acyl-Coa synthetase long-chain; AKR1C: Aldo-keto reductase type 1C; DHODH: dihydroorotate dehydrogenase; FSP1: ferroptosis suppressor protein 1; PUFAs: polyunsaturated fatty acids; GPX: glutathione peroxidase; GSH: glutathione; GST: glutathione-S-transferase; GSS: glutathione synthetase; SHMT: serine hydroxymethyltransferase.

interfere with PUFAs enhancing lipid peroxidation. Together with Fenton's reaction, the iron dependent lipoxygenases (indispensable for ferroptosis) and COX2 accumulated during BPA treatment catalyzing free PUFAs peroxidation (Fig. 6), generating active lipid species that interact with membrane lipids triggering an oxidative chain reaction which leads to severe membrane damage [79]. This fact was also supported by the increasing of MDA, and is related to stimulate ferroptosis [25,80]. Although mitochondrial MnSOD accumulates after 24 h of BPA exposure to alleviate ROS, it could act as a two-sided coin, as produced H_2O_2 is related to the loss of membrane potential, also characteristic of ferroptosis [79]. In addition, the decreasing TSS after the initial shock combined with the starch accumulation after 72 h may suggest a reduced respiration consequence of a mitochondrial affection (as well as chloroplasts) and consequently the acetate in the culture media is mobilized into starch rather than being fully oxidized in mitochondria. The ferroptosis suppressor protein-1 (FSP1), which reduces ubiquinone to ubiquinol, is a key enzyme for avoiding this process [81,82], as increased ubiquinol content reduces lipid peroxidation (Fig. 6). Despite its abundance being close to our detection limit, it could not be found after 24 h of BPA treatment but showed similar abundance than controls after 72 h, reflecting ferroptosis alleviation as supported by physiological and biochemical results, which also coincided with the recovery of cell viability rates. Coincidently, dihydroorotate dehydrogenase (DHODH), which couples the oxidation of dihydroorotate to the reduction of ubiquinone, also mitigating ferroptosis related mitochondrial lipid peroxidation [83], was not detected during initial BPA shock. Moreover other enzymes related to ferroptosis mitigation, as ROS scavenging sulfiredoxin [55] or β-oxidation related Enoyl CoA Hydratase I [84] were enhanced after 24 h of BPA exposure (Fig. 6). On the other hand, aldoketoreductase type 1C (AKR1C), involved in the detoxification of lipidic metabolites during ferroptosis [53] reduced its accumulation at 24 h of BPA exposure, possibly enhancing ferroptosis effects. The rescue of Chlamydomonas growth and the early recovery of BPA-damage biomarkers by Ferrostatin-1, a canonical ferroptosis inhibitor also supported Ferroptosis hypothesis.

The discovery of a ferroptosis process sharing both animal and plant elements demonstrated again the singularity of Chlamydomonas [20] with elements of plant and animal kingdom. Between them, it is remarkably the presence of the Human FSP1 homolog and the role of Malic enzyme, indispensable for plant ferroptosis. However, there are key elements that were missing, as the higher plant characteristic Kiss of Death (KOD) ubiquitin protein, which is indispensable for higher plants ferroptosis occurrence under heat stress [24] or the XC- system, indispensable for mammal ferroptosis which are not present in Chlamydomonas genome [20]. Both the resemblances and differences make the Chlamydomonas ferroptosis a pathway to study to learn the key evolutionary elements between clades.

Behind this cell death response, Chlamydomonas proved themselves a good choice for bioremediation. Not-very dense cultures ($5{\cdot}10^4$ cells/mL) could reduce almost half a high concentration of BPA (40 mg/L) during the first 24 h. This accumulation capacity is remarkable compared to other algae, which were unable to remove BPA with the same efficiency [6], or land plants as tobacco, which were able to accumulate BPA at the cost of a very reduced growth [85].

5. Conclusions

Chlamydomonas reinhardtii was an interesting microalga for bioremediating BPA contamination, as it could grow and accumulate BPA at high concentrations. However, the exposure to BPA was not innocuous for this organism, as it initially altered most of the cellular functions due to redox homeostasis, which was recovered after 72 h of culture. Results demonstrated that among cellular responses, ferroptosis showed as the principal mechanism employed by the cells for survival. This was the first time that it was demonstrated that BPA induces this process in a photosynthetic organism, and the occurrence of this process in eukaryotic microalgae provided a good experimental system for studying the molecular mechanisms of ferroptosis and its evolution. Furthermore, the accumulation and immobilization of high amounts of BPA within Chlamydomonas cells makes this species suitable for bioremediation. However, more research is necessary to fully understand how ferroptosis works in microalgae, focusing on broad responses and key regulators. These findings open the door for new molecular engineering towards minimizing the BPA effect and increasing bioremediation capabilities.

CRediT authorship contribution statement

María Carbó: Conceptualization, Investigation, Formal analysis, Writing – original draft. **Palak Chaturvedi:** Investigation, Resources. **Ana Álvarez:** Investigation. **Daniela Pineda-Cevallos:** Investigation. **Arindam Ghatak:** Investigation. **Pablo Rodríguez: González:** Resources, Methods. **María Jesús Cañal:** Resources. **Wolfram Weckwerth:** Resources. **Luis Valledor:** Supervision, Conceptualization, Investigation, Formal analysis, Writing – original draft. All authors revised final version of the manuscript.

Declaration of Competing Interest

The authors declare that they have no known competing financial interests or personal relationships that could have appeared to influence the work reported in this paper.

Data Availability

Data will be uploaded to public repositories.

Acknowledgements

This work and LV were supported by Ramon y Cajal Programme (RYC-2015-17871, Spanish Ministry of Economy and Competitiveness). MC and AA were generously granted by the BP19-137 (Programa de Ayudas Predoctorales Severo Ochoa, Autonomous Community of Asturias, Spain) and FPU19/01142 (Spanish Ministry of Universities) fellowships, respectively. AG is thankful to the European Union Horizon 2020 Research and Innovation Programme under grant agreement number GA 2020 862–858 (ADAPT). PC is thankful to the Austrian Science Fund (FWF, DerWissenschaftsfonds), Grant agreement number I 5234, for their support.

Environmental Implication

Here we report the acclimation response of the microalgae *Chlamydomonas reinhardtii* to the endocrine disruptive pollutant bisphenol A (BPA). The current research reveals the fundamental acclimation mechanisms induced by BPA in microalgae. Together, we propose this microorganism for plastic components bioremediation, as it can accumulate high amounts of BPA. We highlight the pathways that would be improved for efficient microalgae BPA bioremediation through genetic engineering approach.

Appendix A. Supporting information

Supplementary data associated with this article can be found in the online version at doi:10.1016/j.jhazmat.2023.130997.

References

[1] Xanthos, D., Walker, T.R., 2017. International policies to reduce plastic marine pollution from single-use plastics (plastic bags and microbeads): a review. Mar Pollut Bull. https://doi.org/10.1016/j.marpolbul.2017.02.048.

[2] Naveira, C., Rodrigues, N., Santos, F.S., Santos, L.N., Neves, R.A.F., 2021. Acute toxicity of Bisphenol A (BPA) to tropical marine and estuarine species from

different trophic groups. Environ Pollut. https://doi.org/10.1016/j.envpol.2020.115911.
[3] Ma, Y., Liu, H., Wu, J., Yuan, L., Wang, Y., Du, X., Wang, R., Marwa, P.W., Petlulu, P., Chen, X., Zhang, H., 2019. The adverse health effects of bisphenol A and related toxicity mechanisms. Environ Res 176, 108575. https://doi.org/10.1016/j.envres.2019.108575.
[4] Yamamoto, T., Yasuhara, A., Shiraishi, H., Nakasugi, O., 2001. Bisphenol A in hazardous waste landfill leachates. Chemosphere 42, 415–418. https://doi.org/10.1016/S0045-6535(00)00079-5.
[5] Eio, E., Kawai, M., Ito, M.M., Toda, T., 2015. Biodegradation of bisphenol A by an algal-bacterial system. Environ Sci Pollut Res Int. https://doi.org/10.1007/s11356-015-4693-2.
[6] Nakajima, N., Teramoto, T., Kasai, F., Sano, T., Tamaoki, M., Aono, M., Kubo, A., Kamada, H., Azumi, Y., Saji, H., 2007. Glycosylation of bisphenol A by freshwater microalgae. Chemosphere 69, 934–941. https://doi.org/10.1016/J.CHEMOSPHERE.2007.05.088.
[7] Xiao, C., Wang, L., Hu, D., Zhou, Q., Huang, X., 2019. Effects of exogenous bisphenol A on the function of mitochondria in root cells of soybean (Glycine max L.) seedlings. Chemosphere 222, 619–627. https://doi.org/10.1016/J.CHEMOSPHERE.2019.01.195.
[8] Kanwar, M.K., Xie, D., Yang, C., Ahammed, G.J., Qi, Z., Hasan, M.K., Reiter, R.J., Yu, J.Q., Zhou, J., 2020. Melatonin promotes metabolism of bisphenol A by enhancing glutathione-dependent detoxification in Solanum lycopersicum L. J Hazard Mater 388, 121727. https://doi.org/10.1016/J.JHAZMAT.2019.121727.
[9] Zhang, J., Wang, L., Li, M., Jiao, L., Zhou, Q., Huang, X., 2015. Effects of bisphenol A on chlorophyll fluorescence in five plants. Environ Sci Pollut Res 22, 17724–17732. https://doi.org/10.1007/S11356-015-5003-8/TABLES/5.
[10] Li, X., Wang, L., Shen, F., Zhou, Q., Huang, X., 2018. Impacts of exogenous pollutant bisphenol A on characteristics of soybeans. Ecotoxicol Environ Saf 157, 463–471. https://doi.org/10.1016/J.ECOENV.2018.04.013.
[11] Falcão, V.G.O., de, D., Carneiro, C., Pereira, S.A., da Silva, M.R.D., Candé, A.A., da Cunha Lima, S.T., 2019. Analyzing the toxicity of bisphenol-A to microalgae for ecotoxicological applications. Environ Monit Assess 192, 8. https://doi.org/10.1007/s10661-019-7984-0.
[12] Esperanza, M., Seoane, M., Servia, M.J., Cid, Á., 2020. Effects of Bisphenol A on the microalga Chlamydomonas reinhardtii and the clam Corbicula fluminea. Ecotoxicol Environ Saf. https://doi.org/10.1016/j.ecoenv.2020.110609.
[13] Ben Ouada, S., Ben Ali, R., Leboulanger, C., Zaghden, H., Choura, S., Ben Ouada, H., Sayadi, S., 2018. Effect and removal of bisphenol A by two extremophilic microalgal strains (Chlorophyta). J Appl Phycol 30, 1765–1776. https://doi.org/10.1007/S10811-017-1386-X/TABLES/2.
[14] Nakajima, N., Teramoto, T., Kasai, F., Sano, T., Tamaoki, M., Aono, M., Kubo, A., Kamada, H., Azumi, Y., Saji, H., 2007. Glycosylation of bisphenol A by freshwater microalgae. Chemosphere 69, 934–941. https://doi.org/10.1016/j.chemosphere.2007.05.088.
[15] Zhang, W., Xiong, B., Sun, W.F., An, S., Lin, K.F., Guo, M.J., Cui, X.H., 2014. Acute and chronic toxic effects of bisphenol a on Chlorella pyrenoidosa and Scenedesmus obliquus. Environ Toxicol 29, 714–722. https://doi.org/10.1002/TOX.21806.
[16] Xiao, C., Wang, L., Zhou, Q., Huang, X., 2020. Hazards of bisphenol A (BPA) exposure: A systematic review of plant toxicology studies. J Hazard Mater 384. https://doi.org/10.1016/J.JHAZMAT.2019.121488.
[17] Ben Ouada, S., Ben Ali, R., Leboulanger, C., Ben Ouada, H., Sayadi, S., 2018. Effect of bisphenol A on the extremophilic microalgal strain Picocystis sp. (Chlorophyta) and its high BPA removal ability. Ecotoxicol Environ Saf 158, 1–8. https://doi.org/10.1016/J.ECOENV.2018.04.008.
[18] Duan, L., Chen, Q., Duan, S., 2019. Transcriptional analysis of chlorella pyrenoidosa exposed to bisphenol A. Int J Environ Res Public Heal 16, 1374. https://doi.org/10.3390/IJERPH16081374.
[19] Ji, M.-K., Kabra, A.N., Choi, J., Hwang, J.-H., Kim, J.R., Abou-Shanab, R.A.I., Oh, Y.-K., Jeon, B.-H., 2014. Biodegradation of bisphenol A by the freshwater microalgae Chlamydomonas mexicana and Chlorella vulgaris. Ecol Eng 73, 260–269. https://doi.org/10.1016/j.ecoleng.2014.09.070.
[20] Merchant, S.S., Prochnik, S.E., Vallon, O., Harris, E.H., Karpowicz, S.J., Witman, G. B., Terry, A., Salamov, A., Fritz-Laylin, L.K., Maréchal-Drouard, L., Marshall, W.F., Qu, L.-H., Nelson, D.R., Sanderfoot, A.A., Spalding, M.H., Kapitonov, V.V., Ren, Q., Ferris, P., Lindquist, E., Shapiro, H., Lucas, S.M., Grimwood, J., Schmutz, J., Cardol, P., Cerutti, H., Chanfreau, G., Chen, C.-L., Cognat, V., Croft, M.T., Dent, R., 2007. The Chlamydomonas genome reveals the evolution of key animal and plant functions. Sciences (80-) 318. https://doi.org/10.1126/science.1143609.
[21] Malea, P., Kokkinidi, D., Kevrekidou, A., Adamakis, I.D.S., 2022. The enzymatic and non-enzymatic antioxidant system response of the seagrass cymodocea nodosa to bisphenol-A toxicity. Int J Mol Sci 23, 1348. https://doi.org/10.3390/IJMS23031348.
[22] Aguilera, A., Berdun, F., Bartoli, C., Steelheart, C., Alegre, M., Bayir, H., Tyurina, Y. Y., Kagan, V.E., Salerno, G., Pagnussat, G., Martin, M.V., 2022. C-ferroptosis is an iron-dependent form of regulated cell death in cyanobacteria. J Cell Biol 221. https://doi.org/10.1083/JCB.201911005/212878.
[23] Canizal-García, M., Olmos-Orizaba, B.E., Moreno-Jiménez, M., Calderón-Cortés, E., Saavedra-Molina, A., Cortés-Rojo, C., Canizal-Garc Ia, M., Moreno-Jim Enez, M., Calder On-Cort Es, E., Cort Es-Rojo, C., 2021. Glutathione peroxidase 2 (Gpx2) preserves mitochondrial function and decreases ROS levels in chronologically aged yeast. Free Radic Res 55, 165–175. https://doi.org/10.1080/10715762.2021.1882677.
[24] Distéfano, A.M., López, G.A., Setzes, N., Marchetti, F., Cainzos, M., Cascallares, M., Zabaleta, E., Pagnussat, G.C., 2021. Ferroptosis in plants: triggers, proposed mechanisms, and the role of iron in modulating cell death. J Exp Bot 72, 2125–2135. https://doi.org/10.1093/JXB/ERAA425.
[25] Jiang, X., Stockwell, B.R., Conrad, M., 2021. Ferroptosis: mechanisms, biology and role in disease. Nat Rev Mol Cell Biol 22, 266–282. https://doi.org/10.1038/s41580-020-00324-8.
[26] Bao, L., Zhao, C., Feng, L., Zhao, Y., Duan, S., Qiu, M., Wu, K., Zhang, N., Hu, X., Fu, Y., 2022. Ferritinophagy is involved in Bisphenol A-induced ferroptosis of renal tubular epithelial cells through the activation of the AMPK-mTOR-ULK1 pathway. Food Chem Toxicol 163, 112909. https://doi.org/10.1016/J.FCT.2022.112909.
[27] Colina, F., Carbó, M., Álvarez, A., Meijón, M., Cañal, M.J., Valledor, L., 2020. In: Jorrin-Novo, J.V., Valledor, L., Castillejo, M.A., Rey, M.-D. (Eds.), Multiple Biomolecule Isolation Protocol Compatible with Mass Spectrometry and Other High-Throughput Analyses in Microalgae BT - Plant Proteomics: Methods and Protocols. Springer, US, New York, NY, pp. 11–20. https://doi.org/10.1007/978-1-0716-0528-8_2.
[28] Colina, F.J., Carbó, M., Cañal, M.J., Valledor, L., 2020. A complex metabolic rearrangement towards the accumulation of glycerol and sugars consequence of a proteome remodeling is required for the survival of Chlamydomonas reinhardtii growing under osmotic stress. Environ Exp Bot 180, 104261. https://doi.org/10.1016/j.envexpbot.2020.104261.
[29] Colina, F., Carbó, M., Meijón, M., Cañal, M.J., Valledor, L., 2020. Low UV-C stress modulates Chlamydomonas reinhardtii biomass composition and oxidative stress response through proteomic and metabolomic changes involving novel signalers and effectors. Biotechnol Biofuels 13, 110. https://doi.org/10.1186/s13068-020-01750-8.
[30] Valledor, L., Furuhashi, T., Recuenco-Muñoz, L., Wienkoop, S., Weckwerth, W., 2014. System-level network analysis of nitrogen starvation and recovery in Chlamydomonas reinhardtii reveals potential new targets for increased lipid accumulation. Biotechnol Biofuels 7, 171. https://doi.org/10.1186/s13068-014-0171-1.
[31] Karalija, E., Carbó, M., Coppi, A., Colzi, I., Dainelli, M., Gašparović, M., Grebenc, T., Gonnelli, C., Papadakis, V., Pilić, S., Šibanc, N., Valledor, L., Poma, A., Martinelli, F., 2022. Interplay of plastic pollution with algae and plants: hidden danger or a blessing. ?, J Hazard Mater 438, 129450. https://doi.org/10.1016/J.JHAZMAT.2022.129450.
[32] Yan, C., Qu, Z., Wang, J., Cao, L., Han, Q., 2022. Microalgal bioremediation of heavy metal pollution in water: Recent advances, challenges, and prospects. Chemosphere 286, 131870. https://doi.org/10.1016/J.CHEMOSPHERE.2021.131870.
[33] Nie, J., Sun, Y., Zhou, Y., Kumar, M., Usman, M., Li, J., Shao, J., Wang, L., Tsang, D. C.W., 2020. Bioremediation of water containing pesticides by microalgae: Mechanisms, methods, and prospects for future research. Sci Total Environ 707, 136080. https://doi.org/10.1016/J.SCITOTENV.2019.136080.
[34] López-Hidalgo, C., Meijón, M., Lamelas, L., Valledor, L., 2021. The rainbow protocol: A sequential method for quantifying pigments, sugars, free amino acids, phenolics, flavonoids and MDA from a small amount of sample. Plant Cell Environ 44, 1977–1986. https://doi.org/10.1111/PCE.14007.
[35] MacIntyre, H.L., Cullen, J.J., 2016. Classification of phytoplankton cells as live or dead using the vital stains fluorescein diacetate and 5-chloromethylfluorescein diacetate. J Phycol 52, 572–589. https://doi.org/10.1111/JPY.12415.
[36] Chouhan, N., Devadasu, E., Yadav, R.M., Subramanyam, R., 2022. Autophagy induced accumulation of lipids in pgrl1 and pgr5 of chlamydomonas reinhardtii under high light. Front Plant Sci 12, 3308. https://doi.org/10.3389/FPLS.2021.752634/BIBTEX.
[37] Green, L.S., Rogers, E.E., 2004. FRD3 controls iron localization in arabidopsis. Plant Physiol 136, 2523. https://doi.org/10.1104/PP.104.045633.
[38] Crayton, M.A., 1982. A comparative cytochemical study of volvocacean matrix polysaccharides1. J Phycol 18, 336–344. https://doi.org/10.1111/J.1529-8817.1982.TB03193.X.
[39] Valledor, L., Escandón, M., Meijón, M., Nukarinen, E., Cañal, M.J., Weckwerth, W., 2014. A universal protocol for the combined isolation of metabolites, DNA, long RNAs, small RNAs, and proteins from plants and microorganisms. Plant J. https://doi.org/10.1111/tpj.12546.
[40] Smith, P.K., Krohn, R.I., Hermanson, G.T., Mallia, A.K., Gartner, F.H., Provenzano, M.D., Fujimoto, E.K., Goeke, N.M., Olson, B.J., Klenk, D.C., 1985. Measurement of protein using bicinchoninic acid. Anal Biochem 150, 76–85. https://doi.org/10.1016/0003-2697(85)90442-7.
[41] Chaturvedi, P., Ischebeck, T., Egelhofer, V., Lichtscheidl, I., Weckwerth, W., 2013. Cell-specific analysis of the tomato pollen proteome from pollen mother cell to mature pollen provides evidence for developmental priming. J Proteome Res 12, 4892–4903. https://doi.org/10.1021/PR400197P.
[42] Ghatak, A., Chaturvedi, P., Bachmann, G., Valledor, L., Ramšak, Ž., Bazargani, M. M., Bajaj, P., Jegadeesan, S., Li, W., Sun, X., Gruden, K., Varshney, R.K., Weckwerth, W., 2021. Physiological and proteomic signatures reveal mechanisms of superior drought resilience in pearl millet compared to wheat. Front Plant Sci 11, 1965. https://doi.org/10.3389/FPLS.2020.600278/BIBTEX.
[43] Valledor, L., Weckwerth, W., 2014. An improved detergent-compatible gel-fractionation LC-LTQ-orbitrap-MS workflow for plant and microbial proteomics. In: Jorrin-Novo, J.V., Komatsu, S., Weckwerth, W., Wienkoop, S. (Eds.), Plant Proteomics Methods Protoc. Humana Press, Totowa, pp. 347–358. https://doi.org/10.1007/978-1-62703-631-3_25.
[44] Valledor, L., Recuenco-Munoz, L., Egelhofer, V., Wienkoop, S., Weckwerth, W., 2012. The different proteomes of Chlamydomonas reinhardtii. J Proteom 75. https://doi.org/10.1016/j.jprot.2012.07.045.
[45] R: The R Project for Statistical Computing, (n.d.). https://www.r-project.org/ (Accessed 28 January 2023).

[46] Download RStudio | The Popular Open-Source IDE from Posit, (n.d.). https://posit.co/products/open-source/rstudio/ (Accessed 28 January 2023).
[47] Shannon, P., Markiel, A., Ozier, O., Baliga, N.S., Wang, J.T., Ramage, D., Amin, N., Schwikowski, B., Ideker, T., 2003. Cytoscape: a software environment for integrated models of biomolecular interaction networks. Genome Res 13, 2498. https://doi.org/10.1101/GR.1239303.
[48] Reimand, J., Isserlin, R., Voisin, V., Kucera, M., Tannus-Lopes, C., Rostamianfar, A., Wadi, L., Meyer, M., Wong, J., Xu, C., Merico, D., Bader, G.D., 2019. Pathway enrichment analysis and visualization of omics data using g: Profiler, GSEA, Cytoscape and EnrichmentMap. Nat Protoc 2019 142 (14), 482–517. https://doi.org/10.1038/s41596-018-0103-9.
[49] Lohse, M., Nagel, A., Herter, T., May, P., Schroda, M., Zrenner, R., Tohge, T., Fernie, A.R., Stitt, M., Usadel, B., 2014. Mercator: a fast and simple web server for genome scale functional annotation of plant sequence data. Plant Cell Environ 37, 1250–1258. https://doi.org/10.1111/PCE.12231/SUPPINFO.
[50] Johnson, X., Alric, J., 2012. Interaction between starch breakdown, acetate assimilation, and photosynthetic cyclic electron flow in Chlamydomonas reinhardtii. J Biol Chem 287, 26445–26452. https://doi.org/10.1074/jbc.M112.370205.
[51] Johnson, X., Alric, J., 2013. Central carbon metabolism and electron transport in chlamydomonas reinhardtii: metabolic constraints for carbon partitioning between oil and starch. Eukaryot Cell 12, 776. https://doi.org/10.1128/EC.00318-12.
[52] Valledor, L., Furuhashi, T., Hanak, A.M., Weckwerth, W., 2013. Systemic cold stress adaptation of Chlamydomonas reinhardtiiI. Mol Cell Proteom 12, 2032–2047. https://doi.org/10.1074/MCP.M112.026765/ATTACHMENT/4656EE89-B8C1-4C20-8AC3-9CCC60CAC916/MMC1.ZIP.
[53] Hajdinák, P., Czobor, Á., Szarka, A., 2019. The potential role of acrolein in plant ferroptosis-like cell death. PLoS One 14, e0227278. https://doi.org/10.1371/JOURNAL.PONE.0227278.
[54] Cao, J.Y., Dixon, S.J., 2016. Mechanisms of ferroptosis. Cell Mol Life Sci 73, 2195–2209. https://doi.org/10.1007/S00018-016-2194-1/FIGURES/3.
[55] Chen, X., Li, J., Kang, R., Klionsky, D.J., Tang, D., 2021. Ferroptosis: machinery and regulation. Autophagy 17, 2054. https://doi.org/10.1080/15548627.2020.1810918.
[56] Wu, N.C., Seebacher, F., 2020. Effect of the plastic pollutant bisphenol A on the biology of aquatic organisms: a meta-analysis. Glob Change Biol. 26, 3821–3833. https://doi.org/10.1111/gcb.15127.
[57] Xiao, C., Wang, L., Zhou, Q., Huang, X., 2020. Hazards of bisphenol A (BPA) exposure: a systematic review of plant toxicology studies. J Hazard Mater 384, 121488. https://doi.org/10.1016/J.JHAZMAT.2019.121488.
[58] Qiu, Z., Wang, L., Zhou, Q., 2013. Effects of bisphenol A on growth, photosynthesis and chlorophyll fluorescence in above-ground organs of soybean seedlings. Chemosphere 90, 1274–1280. https://doi.org/10.1016/J.CHEMOSPHERE.2012.09.085.
[59] Li, Y.T., Liang, Y., Li, Y.N., Che, X.K., Zhao, S.J., Zhang, Z.S., Gao, H.Y., 2018. Mechanisms by which Bisphenol A affect the photosynthetic apparatus in cucumber (Cucumis sativus L.) leaves. Sci Rep 2018 81 (8), 1–9. https://doi.org/10.1038/s41598-018-22486-4.
[60] Abu-Ghosh, S., Iluz, D., Dubinsky, Z., Miller, G., 2021. Exogenous abscisic acid confers salinity tolerance in chlamydomonas reinhardtii during its life cycle. J Phycol 57, 1323–1334. https://doi.org/10.1111/JPY.13174.
[61] Yoshida, K., Igarashi, E., Mukai, M., Hirata, K., Miyamoto, K., 2003. Induction of tolerance to oxidative stress in the green alga, Chlamydomonas reinhardtii, by abscisic acid. Plant Cell Environ 26, 451–457. https://doi.org/10.1046/J.1365-3040.2003.00976.X.
[62] Li, S., Wang, P., Zhang, C., Zhou, X., Yin, Z., Hu, T., Hu, D., Liu, C., Zhu, L., 2020. Influence of polystyrene microplastics on the growth, photosynthetic efficiency and aggregation of freshwater microalgae Chlamydomonas reinhardtii. Sci Total Environ 714, 136767. https://doi.org/10.1016/J.SCITOTENV.2020.136767.
[63] Sun, C., Dudley, S., McGinnis, M., Trumble, J., Gan, J., 2019. Acetaminophen detoxification in cucumber plants via induction of glutathione S-transferases. Sci Total Environ 649, 431–439. https://doi.org/10.1016/J.SCITOTENV.2018.08.346.
[64] Rahman, M.S., Kang, K.H., Arifuzzaman, S., Pang, W.K., Ryu, D.Y., Song, W.H., Park, Y.J., Pang, M.G., 2019. Effect of antioxidants on BPA-induced stress on sperm function in a mouse model. Sci Rep 2019 91 (9), 1–10. https://doi.org/10.1038/s41598-019-47158-9.
[65] Zhang, J., Wang, L., Zhou, Q., Huang, X., 2018. Reactive oxygen species initiate a protective response in plant roots to stress induced by environmental bisphenol A. Ecotoxicol Environ Saf 154, 197–205. https://doi.org/10.1016/J.ECOENV.2018.02.020.
[66] Ivanăurovcová, I.I., Goffa, E., Šestáková, Z., Mániková, D., Gaplovská-Kyselá, K., Chovanec, M., Ševčovičová, A., Svetec, I.-K., 2021. Acute exposure to bisphenol A causes oxidative stress induction with mitochondrial origin in saccharomyces cerevisiae cells. J Fungi (Basel). https://doi.org/10.3390/jof7070543.
[67] Bisphenol A inhibits mucin 2 secretion in intestinal goblet cells through mitochondrial dysfunction and oxidative stress | Elsevier Enhanced Reader, (n.d.). https://reader.elsevier.com/reader/sd/pii/S075333221838065X?token=72EDB10375AF7A7D3DBC582ED42A63663CAF97DDDBAAE1ACAF097D7AC31059D2961E9506F38338E86E917A618564280B&originRegion=eu-west-1&originCreation=20220130222547 (Accessed 30 January 2022).
[68] Dayer, R., Fischer, B.B., Eggen, R.I.L., Lemaire, S.D., 2008. The Peroxiredoxin and Glutathione Peroxidase Families in Chlamydomonas reinhardtii. Genetics 179, 41. https://doi.org/10.1534/GENETICS.107.086041.
[69] Barman, A., Hamelberg, D., 2016. Fe(II)/Fe(III) redox process can significantly modulate the conformational dynamics and electrostatics of pirin in NF-Î°B regulation. ACS Omega 1, 837–842. https://doi.org/10.1021/ACSOMEGA.6B00231/SUPPL_FILE/AO6B00231_SI_001.PDF.
[70] Hu, N., Bai, L., Dai, E., Han, L., Kang, R., Li, H., Tang, D., 2021. Pirin is a nuclear redox-sensitive modulator of autophagy-dependent ferroptosis. Biochem Biophys Res Commun 536, 100–106. https://doi.org/10.1016/J.BBRC.2020.12.066.
[71] Urzica, E.I., Casero, D., Yamasaki, H., Hsieh, S.I., Adler, L.N., Karpowicz, S.J., Blaby-Haas, C.E., Clarke, S.G., Loo, J.A., Pellegrini, M., Merchanta, S.S., 2012. Systems and trans-system level analysis identifies conserved iron deficiency responses in the plant lineage. Plant Cell 24, 3921–3948. https://doi.org/10.1105/TPC.112.102491.
[72] Allen, M.D., Del Campo, J.A., Kropat, J., Merchant, S.S., 2007. FEA1, FEA2, and FRE1, encoding two homologous secreted proteins and a candidate ferrireductase, are expressed coordinately with FOX1 and FTR1 in iron-deficient Chlamydomonas reinhardtii. Eukaryot Cell 6, 1841–1852. https://doi.org/10.1128/EC.00205-07.
[73] Narayanan, N.N., Ihemere, U., Chiu, W., Siritunga, D., Rajamani, S., Singh, S., Oda, S., Sayre, R.T., 2011. The iron assimilatory protein, FEA1, from Chlamydomonas reinhardtii facilitates iron-specific metal uptake in yeast and plants. Front Plant Sci 2, 67. https://doi.org/10.3389/FPLS.2011.00067/BIBTEX.
[74] Li, B., Jiang, Y., Wang, T., He, X., Ma, L., Li, B., Li, Y., 2021. Effect of atrazine on accumulation of iron via the iron transport proteins in the midbrain of SD rats. Sci Total Environ 780, 146666. https://doi.org/10.1016/J.SCITOTENV.2021.146666.
[75] Rashidipour, N., Karami-Mohajeri, S., Mandegary, A., Mohammadinejad, R., Wong, A., Mohit, M., Salehi, J., Ashrafizadeh, M., Najafi, A., Abiri, A., 2020. Where ferroptosis inhibitors and paraquat detoxification mechanisms intersect, exploring possible treatment strategies. Toxicol 433– 434, 152407 https://doi.org/10.1016/J.TOX.2020.152407.
[76] Distéfano, A.M., Martin, M.V., Córdoba, J.P., Bellido, A.M., D'Ippólito, S., Colman, S.L., Soto, D., Roldán, J.A., Bartoli, C.G., Zabaleta, E.J., Fiol, D.F., Stockwell, B.R., Dixon, S.J., Pagnussat, G.C., 2017. Heat stress induces ferroptosis-like cell death in plants. J Cell Biol 216, 463–476. https://doi.org/10.1083/JCB.201605110/VIDEO-4.
[77] Dangol, S., Chen, Y., Hwang, B.K., Jwa, N.S., 2019. Iron- and reactive oxygen species-dependent ferroptotic cell death in rice-magnaporthe oryzae interactions. Plant Cell 31, 189–209. https://doi.org/10.1105/TPC.18.00535.
[78] Conlon, M., Dixon, S.J., 2017. Ferroptosis-like death in plant cells. Mol Cell Oncol 4. https://doi.org/10.1080/23723556.2017.1302906.
[79] Kuang, F., Liu, J., Tang, D., Kang, R., 2020. Oxidative damage and antioxidant defense in ferroptosis. Front Cell Dev Biol 8. https://doi.org/10.3389/FCELL.2020.586578.
[80] Feng, H., Stockwell, B.R., 2018. Unsolved mysteries: How does lipid peroxidation cause ferroptosis? PLoS Biol. https://doi.org/10.1371/journal.pbio.2006203.
[81] Doll, S., Freitas, F.P., Shah, R., Aldrovandi, M., Costa Da Silva, M., Ingold, I., Grocin, A.G., Nishida, T., Da Silva, X., Panzilius, E., Scheel, C.H., Mourão, A., Buday, K., Sato, M., Wanninger, J., Vignane, T., Mohana, V., Rehberg, M., Flatley, A., Schepers, A., Kurz, A., White, D., Sauer, M., Sattler, M., Tate, E.W., Schmitz, W., Schulze, A., O'donnell, V., Proneth, B., Popowicz, G.M., Pratt, D.A., Pedro, J., Angeli, F., Conrad, M., 2019. FSP1 is a glutathione-independent ferroptosis suppressor. Nature 575, 693. https://doi.org/10.1038/s41586-019-1707-0.
[82] Liang, D., Deng, L., Jiang, X., 2020. A new checkpoint against ferroptosis. Cell Res 30, 3. https://doi.org/10.1038/S41422-019-0258-0.
[83] Chen, X., Kang, R., Kroemer, G., Tang, D., 2021. Organelle-specific regulation of ferroptosis. Cell Death Differ 2021 2810 (28), 2843–2856. https://doi.org/10.1038/s41418-021-00859-z.
[84] Liu, B., Yi, W., Mao, X., Yang, L., Rao, C., 2021. Enoyl coenzyme A hydratase 1 alleviates nonalcoholic steatohepatitis in mice by suppressing hepatic ferroptosis. Am J Physiol Endocrinol Metab 320, E925–E937. https://doi.org/10.1152/AJPENDO.00614.2020.
[85] Fu, W., Chen, X., Zheng, X., Liu, A., Wang, W., Ji, J., Wang, G., Guan, C., 2022. Phytoremediation potential, antioxidant response, photosynthetic behavior and rhizosphere bacterial community adaptation of tobacco (Nicotiana tabacum L.) in a bisphenol A-contaminated soil. Environ Sci Pollut Res Int. https://doi.org/10.1007/S11356-022-21765-Y.